AGU PUBLICATIONS

JGR

Journal of Geophysical Research: Solid Earth

RESEARCH ARTICLE
10.1002/2015JB012741

Key Points:
- We proposed a physics-based model for granular flow and stick-slip failure on faults
- Vibration advances slip events
- Slip becomes progressively slower upon increase in vibration intensity

Correspondence to:
C. K. C. Lieou,
clieou@lanl.gov

Citation:
Lieou, C. K. C., A. E. Elbanna, and J. M. Carlson (2016), Dynamic friction in sheared fault gouge: Implications of acoustic vibration on triggering and slow slip, *J. Geophys. Res. Solid Earth*, *121*, 1483–1496, doi:10.1002/2015JB012741.

Received 15 DEC 2015
Accepted 19 FEB 2016
Accepted article online 23 FEB 2016
Published online 11 MAR 2016

Dynamic friction in sheared fault gouge: Implications of acoustic vibration on triggering and slow slip

Charles K. C. Lieou[1,2], Ahmed E. Elbanna[3], and Jean M. Carlson[1]

[1]Department of Physics, University of California, Santa Barbara, California, USA, [2]Solid Earth Geophysics Group and Center for Nonlinear Studies, Los Alamos National Laboratory, Los Alamos, NM, USA, [3]Department of Civil and Environmental Engineering, University of Illinois at Urbana-Champaign, Urbana, Illinois, USA

Abstract Friction and deformation in granular fault gouge are among various dynamic interactions associated with seismic phenomena that have important implications for slip mechanisms on earthquake faults. To this end, we propose a mechanistic model of granular fault gouge subject to acoustic vibrations and shear deformation. The grain-scale dynamics is described by the Shear-Transformation-Zone theory of granular flow, which accounts for irreversible plastic deformation in terms of flow defects whose density is governed by an effective temperature. Our model accounts for stick-slip instabilities observed at seismic slip rates. In addition, as the vibration intensity increases, we observe an increase in the temporal advancement of large slip events, followed by a plateau and gradual decrease. Furthermore, slip becomes progressively slower upon increasing the vibration intensity. The results shed important light on the physical mechanisms of earthquake triggering and slow slip and provide essential elements for the multiscale modeling of earthquake ruptures. In particular, the results suggest that slow slip may be triggered by tremors.

1. Introduction

Under high normal stresses a comminuted fault gouge layer forms between rock surfaces on an earthquake fault [*Sammis et al.*, 1987; *Mair and Abe*, 2011; *Lieou et al.*, 2014a]. The characteristics and dynamics of the gouge layer have important implications for the frictional response of the fault under shear. For example, recent experiments have shown that angular, frictional grains display autoacoustic compaction, i.e., the reduction of the granular layer thickness due to internally generated acoustic vibrations[*van der Elst et al.*, 2012; *Dijksman et al.*, 2011; *Wortel et al.*, 2014]. This results in nonmonotonic variation of shear zone layer thickness with shear rate. Our recent theoretical analysis [*Lieou et al.*, 2014b, 2015] suggests that this is a source of instability that is linked to the emergence of stick slip. In stick-slip motion, the stick phase corresponds to the accumulation of strain energy during interseismic periods, while the slip phase corresponds to the occurrence of an earthquake [*Brace and Byerlee*, 1966, 1970; *Johnson et al.*, 1973]. It has been shown that stick slip can be controlled by the imposed strain rate and the confining pressure [*Daub and Carlson*, 2009; *Hayman et al.*, 2011; *Lieou et al.*, 2015], as well as by external vibrations imposed at the boundaries of the granular layer [*Johnson et al.*, 2008; *Griffa et al.*, 2011, 2013; *Ferdowsi et al.*, 2014a, 2014b; *Lieou et al.*, 2015].

In this paper we focus on the effect of varying the vibration intensity on the frictional response of the sheared gouge layer. There are various sources of vibrations in the Earth's crust; these include seismic waves generated by normal earthquakes, ambient noise due to tidal variations and ocean waves, and volcanic as well as nonvolcanic tremors. The latter has triggered immense interest over the past decade since its discovery by *Obara* [2002]. Unlike normal earthquakes which last for a short duration (few seconds to minutes) and have a broadband frequency spectrum, tremors are long-lived, narrowbanded vibrations, mostly in the 1–10 Hz frequency band [*Obara*, 2002]. Nonvolcanic tremors have been observed in many regions including subduction zones as well as strike-slip faults such as the San Andreas Fault [see, e.g., *Rubinstein et al.*, 2010, and references therein]. Because dynamic triggering of earthquakes is an established seismological observation [*Marsan and Lengline*, 2008; *Brodsky and Prejean*, 2005], it is crucial to understand the effects of boundary vibration on a confined granular layer.

Of particular interest is the possible connection between slow slip and tremors, supported by ample evidence for their correlation [*Rubinstein et al.*, 2010; *Beroza and Ide*, 2011; *Johnson et al.*, 2012]. Slow slip has been seen in laboratory experiments and field observations such as *Dragert et al.* [2001], *Rogers and Dragert* [2003],

Obara et al. [2004], *Kaproth and Marone* [2013], and *Johnson et al.* [2012]. Among these, *Kaproth and Marone* [2013] suggests that the transition from unstable to stable frictional behavior limits the slip velocity. *Johnson et al.* [2012] and *Liu and Rice* [2007], for example, suggest that slow slip occurs under lower effective stress conditions or on weak faults, which can be achieved by vibrating the gouge layer. Meanwhile, *Zigone et al.* [2012] asserts that tremors and slow slip events can be triggered by passing seismic waves, and *Wei et al.* [2015] reports the triggering of shallow creep events by other earthquakes. While there has been no direct evidence of tremors triggering slow slip, the causal relation between the two remains unclear at this point.

Here we propose a theoretical model that describes how external vibrations and shear control the configurational state of the gouge layer through granular rearrangements. We show that boundary vibrations can result in significant frictional weakening, thereby clock-advancing large slip events. The degree of clock advance increases with vibration intensity when it is small; at higher vibration intensities the clock advance levels off and subsequently shows a gradual decrease. Moreover, slip becomes progressively slower as the vibration intensity increases; the peak slip rate appears to level off around the vibration intensity at which the extent of clock advancement starts to decrease. Upon the gradual transition to slow slip, the strain energy release occurs gradually, and the stress drop is orders of magnitude slower than at lower vibration intensities. The dependence of frictional rheology and, in turn, slip modes on the vibration intensity may have implications for the brittle-to-ductile transition in the crust.

The rest of this paper is organized as follows. We provide a brief overview of the theoretical model in section 2 and relegate the details to the appendices. Section 3 summarizes model predictions; the geophysical implications of which are discussed in section 4.

2. Model Description

Our model is based on the Shear-Transformation-Zone (STZ) theory of dense granular flow [*Falk and Langer*, 1998, 2011; *Lieou et al.*, 2014a, 2014b, 2015], which attributes plastic deformation to irreversible, local granular rearrangement occurring at loose spots, known as STZs. This approach directly connects macroscopic dynamics to the grain-scale physics of deformation, such as the link between frictional properties of grains and their angularity [*Lieou et al.*, 2015]. The STZ theory has been successfully invoked to reconstruct and explain constitutive friction laws [*Daub and Carlson*, 2010; *Lieou et al.*, 2014a; *Elbanna and Carlson*, 2014] and to show that friction between grains is an essential ingredient for stick-slip instabilities [*Lieou et al.*, 2015]. Here we provide a brief overview of the theoretical elements; for further information, the reader may refer to, e.g., *Lieou et al.* [2015].

Under an applied shear stress, nonaffine granular rearrangements occur at STZs to facilitate deformation and flow. The STZ density Λ in a given granular packing is governed by an effective temperature $\chi \propto \partial V/\partial S_C$, termed the compactivity: $\Lambda = 2e^{-1/\chi}$. The compactivity increases with the free volume in the granular layer; since STZs are spots with excess free volume, this relation implies that an increase in free volume corresponds to an increase in the number of STZs, as one intuitively expects. (The derivation of this relation, analogous to the Boltzmann distribution, is based on the second law of thermodynamics; see, for example, *Falk and Langer* [2011] and *Lieou et al.* [2014b] for details.) Here V is the extensive volume occupied by the granular packing, and S_C is the corresponding configurational entropy; we have chosen units so that χ is dimensionless.

For a given amount of granular material, the compactivity χ measures, in effect, the number of ways that the grains can be packed to occupy the extensive volume V or, in the case of a granular layer, the corresponding thickness h. It therefore increases with the thickness of the granular layer, though for our purposes the quantitative relationship between h and χ need not be explicitly specified. Our preference of using the compactivity χ in place of the thickness h is rooted in the thermodynamic foundations of the theory; χ evolves according to the laws of thermodynamics, which must be obeyed in every physical system. This allows us to derive its temporal evolution directly. The quantity χ is an analog of the thermal temperature, in the sense that the temperature measures the energy content of a given closed system.

Plastic deformation occurs when grains rearrange in an irreversible manner that changes the local topology; that is, when STZs "flip" from a direction unstable with respect to the applied stress to one that is stable. The plastic strain rate $\dot{\gamma}^{\mathrm{pl}}$, which equals the local slip rate v^{loc} divided by the thickness h of the gouge layer,

increases with the density of STZs and the difference between the stress-dependent forward and backward transition rates, and decreases with the fraction of STZs which are stable with respect to the applied stress. Thus,

$$\dot{\gamma}^{\mathrm{pl}} = \frac{4\epsilon_0}{\tau} e^{-1/\chi} R_0 \left[\mathcal{T}(\mu, \chi) - m(\mu, \chi) \right]. \tag{1}$$

Here $\tau = a\sqrt{\varrho_g / p}$ is the inertial time scale whose product with the shear rate is the inertial number [*Jop et al.*, 2006], with a, ϱ_g, and p being the characteristic grain size, grain material density, and confining pressure, respectively. The quantity $\mu = s/p$ is the ratio of shear stress to pressure; that is, the macroscopic friction coefficient. $\mathcal{T}(\mu, \chi) = \tanh(\epsilon_0 \mu / \epsilon_Z \chi)$ measures the rate bias for forward STZ transitions, where ϵ_0 and ϵ_Z are the STZ core and excess volumes normalized by the grain volume a^3. Meanwhile, R_0 is average of the forward and backward STZ transition rates, assumed to be a constant for convenience. The quantity $m(\mu, \chi)$ is the stress-dependent STZ orientational bias, whose full expression can be found in equation (A10) in the appendix. That expression contains a yield stress parameter μ_0, such that in the absence of vibrations, $\dot{\gamma}^{\mathrm{pl}} = 0$ whenever $\mu \mathcal{T}(\mu, \chi) < \mu_0$. On the other hand, $m(\mu, \chi) = \mu_0 / \mu$ when $\mu \mathcal{T}(\mu, \chi) > \mu_0$. Thus, the parameter μ_0 controls the minimum shear strength of an unvibrated granular medium.

Because it is easier to make a loose granular material flow, μ_0 should be a decreasing function of increasing χ; we choose the interpolation

$$\mu_0 = \mu_1 + \mu_2 e^{1/\chi}. \tag{2}$$

We argued in *Lieou et al.* [2015] that a minimum shear strength μ_0 that decreases with increasing compactivity χ is one of the necessary ingredients for apparent rate weakening in the slip rate regime where the variation of χ and the layer thickness with the imposed loading rate is nonmonotonic. Note that equation (2) is simply a lower bound for the dynamic friction in terms of the compactivity χ; it is *not* a constitutive friction law. The variation of macroscopic friction with control parameters is to be computed by incorporating this and other physical elements and solving the differential equations of motion.

The complete constitutive description consists of two dynamical equations, one for the shear stress-to-pressure ratio μ and one for the compactivity χ. The equation for μ is a statement of linearity between increments in stress and elastic strain. Thus,

$$\dot{\mu} = (G/p)(\dot{\gamma} - \dot{\gamma}^{\mathrm{pl}}), \tag{3}$$

where G is the aggregate shear modulus, and the imposed shear rate $\dot{\gamma} = v/h$ equals the interfacial relative velocity, or imposed loading rate v, divided by the width h of the gouge layer.

Meanwhile, the equation for χ takes the form

$$\epsilon_1 \dot{\chi} = \mu \dot{\gamma}^{\mathrm{pl}} + \frac{Y}{\tau} - \mathcal{K}(\chi)\chi, \tag{4}$$

where ϵ_1 is a dimensionless, effective volumetric expansion coefficient. Equation (4) is entirely a consequence of the laws of thermodynamics; it says that the compactivity changes at a rate proportional to the rate of plastic work of shear deformation $\mu \dot{\gamma}^{\mathrm{pl}}$ and the rate at which energy Y/τ is delivered into the layer by external acoustic vibrations, minus the rate at which work flows away from the granular layer in the form of entropy loss to the surroundings. The transport coefficient $\mathcal{K}(\chi)$ that describes this loss of entropy must be nonnegative, as a consequence of the second law of thermodynamics. In the appendix we discuss how we identify the work rate Y/τ due to external vibrations and the transport coefficient $\mathcal{K}$ in terms of the sources of noise—loosely interpreted as the jiggling motion of grains. These include the mechanical noise $\Gamma = \tau \mu \dot{\gamma}^{\mathrm{pl}} / (\epsilon_0 \mu_0 \Lambda)$ induced by shearing; the noise induced by external vibrations, characterized by the dimensionless intensity ρ, which is proportional to its amplitude and the square of the vibration frequency [*Knight et al.*, 1995; *Nowak et al.*, 1998]; and the noise ξ induced by frictional contact between grains. Once this is done, equation (4) is cast into the (not-so-elegant) form

$$\dot{\chi} = \frac{2\epsilon_0 \mu_0 e^{-1/\chi}}{\tau \epsilon_1} \left[\Gamma \left(1 - \frac{\chi}{\widehat{\chi}(q)} \right) - \xi \frac{\chi}{\widehat{\chi}(q)} \right] + \frac{A_0 \rho}{\tau \epsilon_1} \left[1 - \exp\left(-\frac{q^2}{\rho} \right) \frac{\chi}{\widetilde{\chi}(\rho)} \right]. \tag{5}$$

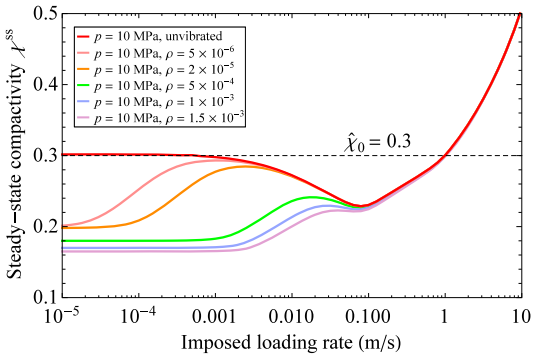

Figure 1. The steady state compactivity χ^{ss} as a function of the imposed loading rate, at lower confining stresses, offers an important hint on the transition from stick slip to slow slip upon increasing the vibration intensity ρ. In the absence of external vibration, there is a pronounced nonmonotonicity in the variation of χ^{ss} with the imposed loading rate, which signifies instabilities. Stick-slip instabilities occur in the shear rate regime where the "dip" appears. As ρ increases, the dip becomes less pronounced. This reduces the propensity for strong rate weakening which is a necessary condition for stick slip; in other words, rate strengthening sets in quickly as one increases the loading rate, to limit the maximum possible local slip rate from above. Slow slip occurs as a result—there is still stick slip, but the stress drop during the slip phase occurs much more gradually. As ρ increases even further, the dip disappears, and steady sliding ensues.

In essence, equation (5) describes how the mechanical noise Γ and the vibrational noise ρ drive the system toward different configurational steady states, described, respectively, by $\hat{\chi}(q)$ and $\tilde{\chi}(\rho)$, and how the friction-induced noise ξ causes further dissipation and compaction [*Lieou et al.*, 2015] upon shearing.

We argued in *Lieou et al.* [2015] that the noise ξ generated by interparticle friction causes the nonmonotonic variation of the layer thickness and the steady state compactivity χ^{ss} with the loading rate v which, along with a μ_0 that decreases with χ, gives rise to possible rate weakening and stick-slip instabilities. More precisely, a nonzero noise strength ξ corresponding to friction provides a means to reduce the compactivity χ to below $\hat{\chi}_0$ for a range of slip rates. In this χ regime, the yield stress parameter μ_0 rapidly decreases with increasing χ, promoting unstable flow. In order for this to happen, ξ should decrease faster than the slip rate in the quasi-static regime, while saturating in the fast, inertial regime so as to not overwhelm the dilation of the granular layer at large strain rates. This is corroborated by the observations of *van der Elst et al.* [2012] on angular quartz sand, and our analysis *Lieou et al.* [2014b] of that experiment.

To interpolate between the fast and slow regimes, it is convenient to choose

$$\xi = \xi_0 \tanh\left[(\tau_f \dot{\gamma}^{pl})^2\right]. \tag{6}$$

Here ξ_0 denotes the maximum noise strength generated by friction, and τ_f is the associated frictional time scale. Note that the nonmonotonic variation of the layer thickness and the key qualitative results presented in this paper are not sensitive to the specific choice of the hyperbolic tangent function. Rather, they arise from the underlying interaction between adjacent grains that give rise to a transition between a saturating frictional noise strength in the fast regime, and a vanishing one in the slow regime, as discussed above.

Then χ^{ss} can be computed directly by setting the left-hand side of equation (5) equal to zero. This is depicted in Figure 1, for a range of vibration intensities ρ, and at pressure $p = 10$ MPa, just below that needed for stick slip to occur [*Lieou et al.*, 2015]. One sees from Figure 1 that the degree of nonmonotonic variation decreases with increasing ρ. Thus, the apparent rate weakening is suppressed; this lowers the maximum possible local

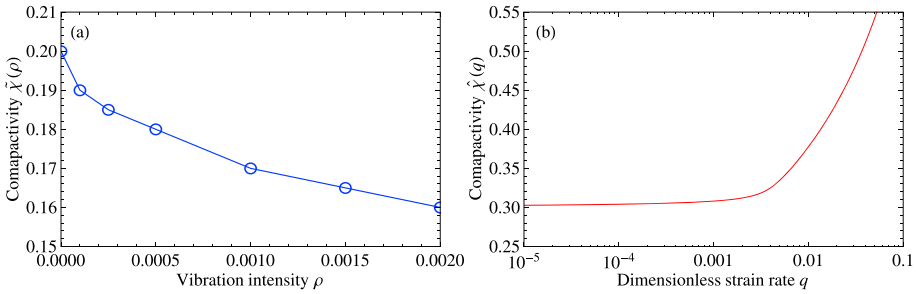

Figure 2. Isolating the effects of shear and vibration. (a) The compactivity $\tilde{\chi}(\rho)$ as a function of vibration intensity ρ, when the granular layer is vibrated but not sheared. (b) The compactivity $\hat{\chi}(q)$ as a function of the dimensionless plastic strain rate $q \equiv \tau\dot{\gamma}^{pl}$, when the granular layer is composed of smooth, frictionless beads and is sheared but not vibrated.

Table 1. List of Parameter Values in the STZ Model[a]

Parameter	Description	Value	Equation
μ_1	Yield stress parameter	0.3	(2)
μ_2	Yield stress parameter	3.7×10^{-3}	(2)
a	Grain size	3.5×10^{-4} m	τ in (1)
ϱ_g	Grain material density	1600 kg/m^3	τ in (1)
R_0	Characteristic STZ transition rate	1	(1)
A_0	Ratio between vibration intensity and corresponding work rate	0.01	(5)
ξ_0	Maximum frictional noise strength	4×10^{-3}	(6)
τ_f	Frictional time scale	1.29×10^{-2} s	(6)
G	Aggregate shear modulus	109 MPa	(3)
$\hat{\chi}_0$	Steady state compactivity as $q \to 0$	0.3	$\hat{\chi}(q)$ in (5)
ϵ_0	Plastic core volume per STZ in units of grain volume	1.5	(1)
ϵ_Z	Excess volume per STZ in units of grain volume	0.5	(1)
ϵ_1	Effective volume expansion coefficient	0.3	(5)

[a]Most of these parameters are identical to those in *Lieou et al.* [2015] and identical to our analysis [*Lieou et al.*, 2014b] of the experiments by *van der Elst et al.* [2012] for angular quartz sand.

slip rate, causing the gradual transition from stick slip to slow slip at higher vibration intensities. At even higher vibration intensities, the nonmonotonic variation of χ^{ss} with v disappears, so that steady sliding takes place at long enough times.

We conclude this section by briefly discussing the quantities $\hat{\chi}(q)$ and $\tilde{\chi}(\rho)$, which appear in equation (5), and are needed to compute the response of the granular layer to shearing and vibration, such as illustrated in Figure 1. Experiments on smooth spherical beads, such as those by *van der Elst et al.* [2012] and *Wortel et al.* [2014], suggest that the degree of dilation of the granular layer increases with shear rate; thus, $\hat{\chi}(q)$ is an increasing function of the dimensionless strain rate $q \equiv \tau \dot{\gamma}^{pl}$. It approaches some constant $\hat{\chi}_0$ as $q \to 0$ and diverges as $q \to \infty$. Its full functional form is discussed in *Lieou et al.* [2014b] and Appendix C and depicted in Figure 2a. On the other hand, the layer thickness is reduced by increasing the vibration intensity ρ; thus, $\tilde{\chi}(\rho)$ is a decreasing function of ρ, our choice of which is depicted in Figure 2b.

3. Results

Equations (3) and (5) are numerically integrated, using an adaptive time-stepping scheme, to solve for the evolution of the shear stress as a function of time, for a range of imposed loading rates $v = \dot{\gamma} h$ and normal

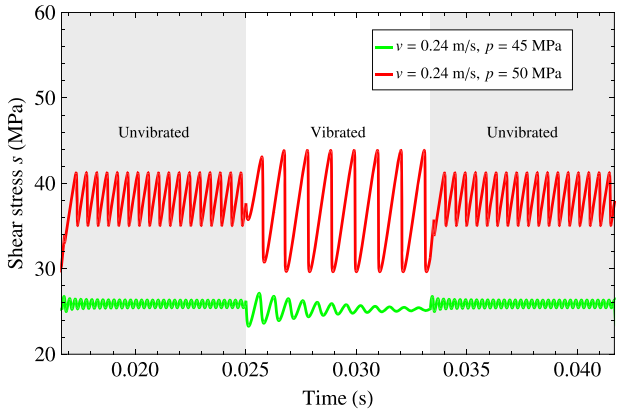

Figure 3. Vibration controls stick-slip behavior in different parameter regimes; it can amplify stick slip or suppress it altogether after a transient. Shown here are two sample stress-slip curves, with external vibration of fixed intensity $\rho = 5 \times 10^{-4}$ switched on and off alternately, as indicated by the grey and white shades. The red curve for $v = 0.24$ m/s and $p = 50$ MPa has been offset by 10 MPa upward for clarity.

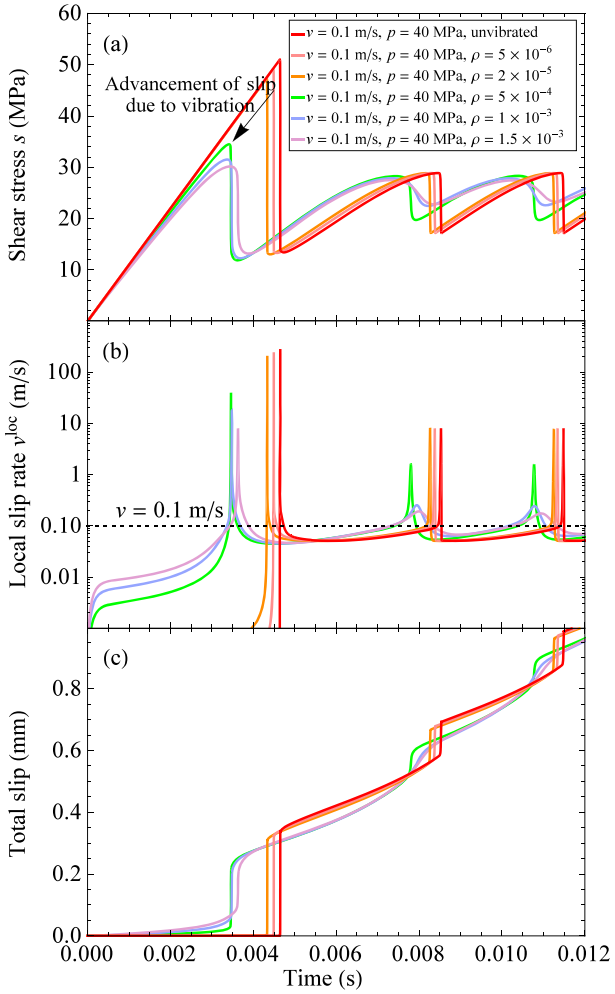

Figure 4. Vibration triggers slip and slow slip. (a) Variation of stress with time, for a range of vibration intensities ρ. The imposed loading rate is $v = 0.1$ m/s, and the confining pressure is $p = 40$ MPa. For direct comparison we also plot in red the stress-slip response for an unvibrated gouge layer. It is seen that vibration advances the onset of the first large slip event and that the extent of clock advance is nearly independent of the vibration intensity as long as $\rho > 5 \times 10^{-4}$. Below this intensity, the clock advancement of the first slip event is less pronounced. When $\rho > 1.5 \times 10^{-3}$, the amount of clock advance decreases slowly. In all cases creep occurs during the stick phase; at higher vibration intensities the stress drop occurs gradually rather an abruptly, and this is a hallmark of slow slip. (b) Variation of local slip rate $v^{\mathrm{loc}} = h\dot{\gamma}^{\mathrm{pl}}$ with time. The imposed loading rate $v = 0.1$ m/s is depicted by the horizontal dotted line for reference. The plot shows that vibration causes slip immediately after the initial loading, before the first large slip event. The slip rate remains nonzero even during the stick phase, and the peak slip rate exceeds the imposed loading rate by less than 1 order of magnitude if ρ is large enough. This is reminiscent of slow slip events. (c) Total, accumulated slip as a function of time. It is seen that creep does indeed occur during the slip phase. In addition, the light blue and light magenta curves show that the slip distance increases slowly, rather than abruptly, when slow slip occurs.

stresses p. The layer thickness is $h = 1$ mm. The initial condition is $\mu(t = 0) = 0.001$ and $\chi(t = 0) = 0.18$. The choice of parameters, motivated by the *van der Elst et al.* [2012], is summarized in Table 1.

Figure 3 shows the effect of switching on and off fixed-intensity vibration in sheared angular grains. For the two sets of imposed loading rate and normal stress values shown ($v = 0.24$ m/s, and $p = 45$ and 50 MPa), boundary vibration can either amplify the stick-slip amplitude, in the case of $p = 50$ MPa, or attenuate stick slip after several decaying cycles, in the case of $p = 45$ MPa. The initial transients upon the onset or cessation of vibration may exhibit effects that differ from the long-time behavior. Specifically, in the case of $p = 50$ MPa, a small stress drop occurs upon switching on or off external vibration, and the stick-slip amplitude approaches that of the limit cycle after a short transient. We shall show below that in other parameter regimes,

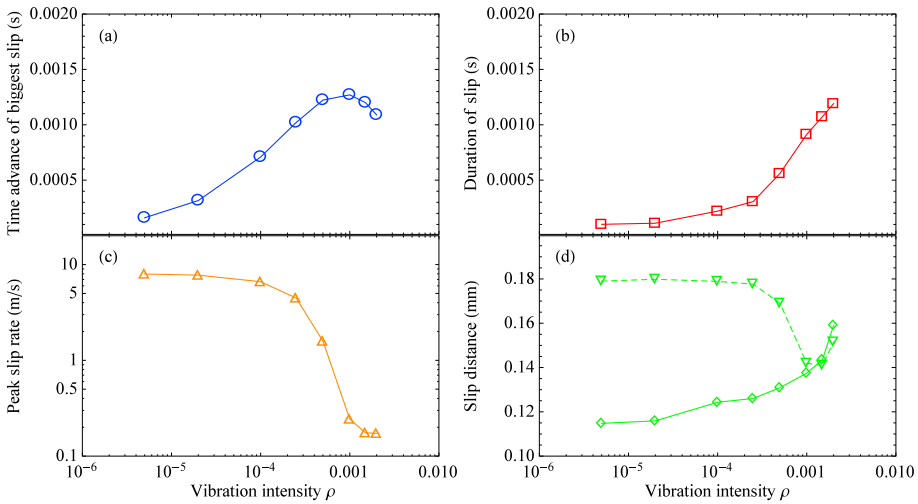

Figure 5. Effect of vibration intensity on slip advancement and slow slip. (a) The degree of time advancement of the first catastrophic slip event upon loading, indicated by the black arrow in Figure 4a, increases rapidly with increasing vibration intensity ρ when $\rho < 0.0005$. It levels off and slightly decreases at higher vibration intensities, which amplify the creep upon loading. (b) The duration of slip in each stick-slip cycle, defined in the text, increases with increasing vibration intensity. (c) The peak slip rate decreases sharply with increasing vibration intensity ρ and becomes comparable to the imposed loading rate $v = 0.1$ m/s around the value of ρ at which the clock advancement of the first large slip event, shown in Figure 5a, starts to slightly decrease. (d) The slip distance during the slip phase in each stick-slip cycle, indicated by diamonds and the solid curve, increases slowly with increasing vibration intensity. It approaches the creep distance—the slip distance accumulated during the stick phase, indicated by inverted triangles and the dashed curve—once the vibration intensity becomes large enough.

boundary vibration may have the opposite effect of reducing the stick-slip amplitudes. In either case, this is a manifestation of the notion that seismic waves emanating from elsewhere can influence stick-slip behavior and, more broadly, seismic events.

The effect of varying the vibration intensity ρ is shown in Figure 4. One sees from Figure 4a that vibration triggers slip. The extent of clock advancement of the large slip event, measured by the temporal shift of the peak stress relative to the unvibrated case, increases with the vibration intensity ρ when it is small. The clock advancement becomes nearly independent of ρ when it exceeds 5×10^{-4} and in fact slightly decreases above $\rho = 10^{-3}$. This observation is summarized in Figure 5a and is qualitatively very similar to that of the discrete element simulations of *Ferdowsi et al.* [2014a, 2014b].

In all cases, creep occurs during the stick phase. Moreover, the stress buildup slows down before the stress drop. According to equation (3), this is an indication of preseismic slip, which was associated with acoustic emissions in *Johnson et al.* [2008]. Indeed, one sees from Figure 4b that the local slip rate v^{loc} is slow but nonzero even during the stick phase; moreover, Figure 4c shows that the slip accumulated during the stick phase is nonzero. In addition to this, preseismic slip occurs almost immediately upon initial loading, in vibrated angular sand, if ρ is large enough. These observations suggest that vibration of high enough intensity triggers slip.

Of interest is the observation that for vibration intensities $\rho = 10^{-3}$ and 1.5×10^{-3}, corresponding to the blue and purple curves in Figure 4a, the stress drop occurs gradually rather than abruptly. This is a hallmark of slow slip [*Johnson et al.*, 2012]. Indeed, Figure 4b shows that unlike for weaker vibration intensities for which the peak local slip rate v^{loc} could be several orders of magnitude larger than the imposed loading rate v; for $\rho = 10^{-3}$ and 1.5×10^{-3}, the peak slip rate exceeds the imposed loading rate by less than 1 order of magnitude. The corresponding curves in Figure 4c for total slip as a function of time shows that slip occurs gradually, rather than abruptly, for these vibration intensities. This suggests that boundary vibration of strong enough intensity and, more broadly, seismic waves of large enough amplitude, may constitute a slow slip mechanism [*Rubinstein et al.*, 2010]. As an aside, note from Figures 4a that fixed-intensity vibration reduces the magnitude of stress drop in each stick-slip cycle. This stands in contrast to the case $v = 2.4$ m/s shown in Figure 3 above, for which vibration amplifies the stick-slip amplitude. For even higher vibration intensities,

stick slip can disappear altogether and steady sliding ensues. This could, in fact, be inferred from Figure 1, which shows that the nonmonotonicity in the variation of steady state shear zone thickness becomes less pronounced as ρ increases, reducing the propensity for strong rate weakening which is a necessary condition for stick slip.

These observations regarding the effect of vibration intensity ρ on slip advancement and slow slip are summarized in Figure 5. In Figure 5a we show the variation of the degree of time advance of the first large slip event upon loading, defined previously as the temporal shift of the peak stress relative to the unvibrated case and denoted by the black arrow in Figure 4a, with the vibration intensity ρ. We see that the extent of clock advance increases with increasing vibration intensity below $\rho = 5 \times 10^{-4}$. At larger ρ, it gradually levels off and slightly decreases, as vibration of high enough intensity softens the material and results in creep. Figure 5b shows that the duration of slip in each stick-slip cycle, defined as the time elapsed between a stress peak and the subsequent minimum, increases as a function of ρ. This implies that slip becomes slower as the vibration intensity ρ increases. This is corroborated by Figure 5c which shows that the peak slip rate in each stick-slip cycle drops dramatically with increasing vibration intensity. Both of these are effects that can also be seen from Figure 4b. Interestingly, a direct comparison of Figures 5a and 5c shows that the peak slip rate appears to level off around the vibration intensity $\rho \approx 1.5 \times 10^{-3}$ at which the clock advancement of the first large slip event upon loading starts to slowly decrease. Finally, Figure 5d shows that the slip distance during the slip phase in each stick-slip cycle increases only slightly with vibration intensity. Still, it exceeds the creep distance—the slip distance during the stick phase in each stick-slip cycle—once the vibration intensity is large enough to facilitate the gradual transition into slow slip.

4. Discussion

In this paper we have proposed a mechanistic model for the deformation and flow of a sheared granular layer. The STZ model attributes granular flow to local, irreversible rearrangement of grains at loose spots, and seeks to quantify the propensity for nonaffine rearrangement through an effective temperature termed the compactivity. Based on laws of nonequilibrium thermodynamics, we can deduce how the stress state and the compactivity evolve with time. The model naturally accounts for the effects of boundary vibration and interparticle friction through associated noise strengths.

Among the key results, we have shown that boundary vibration triggers slip. Specifically, as the vibration intensity ρ increases, there is a rapid and almost linear increase in the extent of clock advancement of slip. As ρ increases further, the extent of slip advancement levels off and gradually decreases. For these vibration intensities we observe stick-slip cycles with increasingly slow slip; the peak slip rate in each slow slip event exceeds the imposed loading rate by less than 1 order of magnitude, and certainly much lower than the peak slip rate in each stick-slip cycle. At even higher vibration intensities, there is a transition from stick slip to steady sliding, which coincides with the absence of instability in Figure 1.

The vibration intensity can be computed directly from the vibration amplitude and frequency, or the so-called acoustic strain amplitude [*van der Elst et al.*, 2012]. Vibration controls the stress drop magnitude in each stick-slip cycle and can cause the cessation of stick slip altogether after some transient, depending on the imposed loading rate and the confining pressure. These predictions are in qualitative agreement with computer simulations such as *Johnson et al.* [2008], *Ferdowsi et al.* [2014a, 2014b], and *Tordesillas et al.* [2009]. Here we have mostly considered vibration of fixed intensity ρ over time. The effect of a time-varying vibration intensity, or one of a duration that is short compared with the slip duration, would be the subject of a forthcoming study.

For the range of vibration intensities considered in this paper, the duration of slip increases by about an order of magnitude upon increasing the vibration intensity. A further increase in vibration intensity is expected to lengthen the slip duration even more due to the gradual transition from nonmonotonic friction rheology to a monotonic one (Figure 1). It is thus not difficult to imagine that slip duration several orders of magnitude longer than dynamic slip is realizable within our model. Note that the vibration intensity is proportional to the product of vibration amplitude and square of vibration frequency. Thus, an increase in vibration intensity may correspond to seismic waves of larger amplitude or higher frequency. While dynamic triggering of normal earthquakes by other earthquakes has been documented, our model suggests that high vibration intensities, as exemplified by the high-frequency waves of a tremor swarm, may result in triggered slow slip.

Slow slip events triggered by passing seismic waves has been documented before [e.g., *Itaba and Ando*, 2011; *Zigone et al.*, 2012; *Wei et al.*, 2015], but future seismological observations may be able to validate our hypothesis that slow slip can be triggered by tremors.

Nonvolcanic tremors usually occur beneath the seismogenic zone although their precise location is still a matter of debate. Our observation that stick-slip instabilities are suppressed if the vibration intensity is above some threshold may imply that seismic events can penetrate deeper in regions where tremors are absent. This may be verified by additional seismological observations and by constructing an extended, two-dimensional version of the present model in which the vibration intensity varies with depth.

Slow slip is possible within our model for a range of vibration intensities. There are several theoretical models for slow slip in the literature. These include a rate-and-state fault under nearly lithostatic pore pressures [*Liu and Rice*, 2007], stabilization by fault gouge dilatancy that result in a reduction in pore fluid pressure and slip arrest [*Rubin*, 2008], and a stochastic Brownian fault model [*Ide*, 2008]. Our model provides a new hypothesis for another possible mechanistic origin of slow slip, in addition to those in the literature, by emphasizing the role of externally and internally generated vibrations in regulating the stability of frictional sliding. It allows for the possibility that high-frequency oscillations, such as the high-frequency components of tremor swarms, may trigger slow slip. This is in addition to other slow-slip triggering mechanisms such as seismic waves from earthquakes occurring elsewhere, well documented in the literature. (Here we make explicit the distinction between tremors and seismic waves as possible causes of triggered slow slip; the application of boundary vibrations over an extended period of time mimics long-lived tremor swarms closely and may be related to observations that tremors and slow slip occur at the same time in the same fault region. What triggers tremors is another question, and indeed, normal earthquakes may trigger tremors.)

Furthermore, our model is fully consistent with the laws of thermodynamics. The value of a physics-based model, such as the one discussed in this paper, lies in its ability to offer a predictive description of phenomena that may occur at regimes which are not currently accessible by laboratory experiments. The STZ model offers a unified understanding of the underlying mechanisms for stick-slip failure, preseismic slip, triggering of slip and slow slip, and the amplification and suppression of catastrophic seismic events that involve the presence of a gouge layer.

In particular, while the dominant viewpoint is that tremors emerge as collective slow slip, our model suggests that tremors, which may be caused by other sources, trigger slow slip in turn. This is a hypothesis that can be tested in the laboratory. Thus, a mechanistic model of this type, which incorporates the various grain-scale physical processes involved, constitutes an important step toward developing a more realistic and robust constitutive description of fault friction. Such a description is an essential ingredient in dynamic rupture models.

It has been suggested that slow slip associated with a nonvolcanic tremor must occur when the fault is near its critical state [*Gomberg*, 2010; *Johnson et al.*, 2008; *Scholz*, 2010]. Characterization of the stress state immediately preceding triggered slip or slow slip, as well as the degree to which preseismic slip hints at the approach of stress drop associated with normal or slow slip events, may have major implications on seismic hazard prediction.

The choice of material parameters in our model is motivated by the *van der Elst et al.* [2012] experiments. Those experiments were carried out at a low confining pressure of $p = 7$ kPa; there is no evidence that the parameters extracted from the experiments can be carried over to the seismic regime or otherwise. Rather, our goal is to investigate the consequences of directly extrapolating from laboratory experiments to the seismic regime. As such, several interesting observations regarding the role of acoustic vibration have been made in this regard and discussed in this paper. Further simulations, experiments, and observations in different parameter regimes would be useful in constraining the dependencies of material parameters such as the minimum flow stress μ_0 and the frictional noise strength ξ on the pressure and the imposed loading rate, enabling a more robust extrapolation and application of the theory to the seismic regime.

In this paper we assumed for simplicity that the gouge layer is spatially homogeneous, as is the vibration intensity. In reality, a granular medium is heterogeneous in all spatial directions. The shear-banding instability, which can be produced by a spatially heterogeneous compactivity distribution [*Manning et al.*, 2007, 2009; *Daub and Carlson*, 2009; *Lieou et al.*, 2014a], may need to be invoked to fully describe the irregular stick-slip dynamics seen in experiments such as *Johnson et al.* [2008]. In addition, seismic waves attenuate

upon propagating through a fault, and the corresponding vibration intensity may depend on the location. These ingredients may need to be incorporated to model slips and earthquake ruptures that may occur at different locations along a fault.

Several studies [e.g., *Ferdowsi et al.*, 2014a, 2014b; *Griffa et al.*, 2011] have shown that nonlinear hysteretic phenomena, such as the slow relaxation upon the cessation of boundary vibrations, or in an unsheared gouge layer, can occur. To fully capture these observations, new ingredients such as physics at grain contacts may need to be added to the STZ model. Further delineation of these phenomena within our framework may shed light on the metastability of the earthquake fault and the associated ground motion on different time scales.

Appendix A: Mechanistic Aspects of the STZ Model for Granular Flow

A granular material flows because of irreversible granular rearrangements; these events occur at rare, non-interacting soft spots with excess free volume, known as shear transformation zones or STZs. Given an STZ and an applied shear stress, one can in most cases tell whether granular rearrangement can occur at the STZ, or whether the direction of the applied shear stress impedes the rearrangement of grains. Thus, the applied shear stress defines a direction relative to which STZs can be classified according to orientation, with total numbers N_+ and N_-, respectively. If the shear stress is in the "plus" direction, minus-type STZs readily flip or transition to become plus type. Plus-type STZs, however, rarely flip; instead, they are annihilated readily by noise, which can also create STZs elsewhere. This process is described by the master equation

$$\tau \dot{N}_{\pm} = \mathcal{R}(\pm\mu, \chi) N_{\mp} - \mathcal{R}(\mp\mu, \chi) N_{\pm} + \tilde{\Gamma}(N^{\mathrm{eq}}/2 - N_{\pm}). \tag{A1}$$

Here $\tilde{\Gamma} = \Gamma + \rho$, the sum of the mechanical (i.e., associated with shearing) and vibrational noise strengths, is the rate (in units of the inverse time scale $1/\tau$) at which STZs are created and annihilated. As discussed in the main paper, the time scale τ is conveniently chosen to be the inertial time scale $\tau = a\sqrt{\rho_G/p}$, where a, ρ_G, and p are the characteristic grain size, grain material density, and pressure. Note that the noise due to frictional contact between particles ξ does not enter into equation (A1), because friction between grains dissipates energy but does not open up or close voids.

If N is the total number of grains, the plastic strain rate is given by

$$\dot{\gamma}^{\mathrm{pl}} = \frac{2\epsilon_0}{\tau N} \left[\mathcal{R}(\mu, \chi) N_- - \mathcal{R}(-\mu, \chi) N_+ \right]. \tag{A2}$$

Once we introduce the intensive variables

$$\Lambda = \frac{N_+ + N_-}{N}; \quad m - \frac{N_+ - N_-}{N_+ + N_-}, \tag{A3}$$

which represent the density and orientational bias of STZs, as well as the combination of the forward and backward transition rates

$$\mathcal{C}(\mu, \chi) = \frac{1}{2} \left[\mathcal{R}(\mu, \chi) + \mathcal{R}(-\mu, \chi) \right]; \tag{A4}$$

$$\mathcal{T}(\mu, \chi) = \frac{\mathcal{R}(\mu, \chi) - \mathcal{R}(-\mu, \chi)}{\mathcal{R}(\mu, \chi) + \mathcal{R}(-\mu, \chi)}, \tag{A5}$$

the expression for the plastic strain rate, equation (A2), can be written as

$$\dot{\gamma}^{\mathrm{pl}} = \frac{2\epsilon_0 \Lambda}{\tau} \mathcal{C}(\mu, \chi)[\mathcal{T}(\mu, \chi) - m], \tag{A6}$$

which is the same as equation (1) in the main paper, once we identify the STZ density as $\Lambda = 2e^{-1/\chi}$ below, and use the approximation that $\mathcal{C}(\mu, \chi) \approx R_0$ for some constant R_0, whenever μ is not too large.

Meanwhile, equation (A1) can be recast in terms of Λ and m as

$$\tau \dot{\Lambda} = \tilde{\Gamma}(\Lambda^{\mathrm{eq}} - \Lambda); \tag{A7}$$

$$\tau \dot{m} = 2\mathcal{C}(\mu, \chi)[\mathcal{T}(\mu, \chi) - m] - \tilde{\Gamma} m - \tau \frac{\dot{\Lambda}}{\Lambda} m. \tag{A8}$$

Because STZs are rare and noninteracting, $\Lambda \ll 1$. The equations for $\dot{\Lambda}$ and $\dot{m}$ above do not contain the small factor Λ, but the expression for the plastic strain rate, (A6), does. As a result, Λ and m equilibrate on a much faster time scale — plausibly a layer thickness divided by the inverse sound speed — than the other dynamical variables. Thus, it suffices to replace Λ and m from now on by their stationary values, i.e., the values for which $\dot{\Lambda} = \dot{m} = 0$.

It follows that we can replace Λ by Λ^{eq} everywhere; application of the second law of thermodynamics yields $\Lambda^{\mathrm{eq}} = 2e^{-1/\chi}$ and also gives $\mathcal{T}(\mu, \chi) = \tanh(\epsilon_0 \mu / \epsilon_Z \chi)$. (The complete argument is somewhat lengthy and is beyond the scope of the present paper; the interested reader may refer to, for example, *Lieou et al.* [2015] for details.) Meanwhile, to compute m^{eq}, note that the mechanical noise strength is proportional to the energy dissipated per STZ; thus,

$$\Gamma = \frac{\tau \mu \dot{\gamma}^{\mathrm{pl}}}{\epsilon_0 \mu_0 \Lambda^{\mathrm{eq}}} = \frac{2\mu}{\mu_0} R_0 [\mathcal{T}(\mu, \chi) - m], \tag{A9}$$

where μ_0 is a stress scale whose significance will become evident shortly. This can be substituted into the equation for $\dot{m}$, equation (A8), whose stationary version becomes

$$2R_0 [\mathcal{T}(\mu, \chi) - m] \left(1 - \frac{m\mu}{\mu_0}\right) - m\rho = 0, \tag{A10}$$

so that

$$m^{\mathrm{eq}} = \frac{\mu_0}{2\mu} \left[1 + \frac{\mu}{\mu_0} \mathcal{T}(\mu, \chi) + \frac{\rho}{2R_0}\right] - \frac{\mu_0}{2\mu} \sqrt{\left[1 + \frac{\mu}{\mu_0} \mathcal{T}(\mu, \chi) + \frac{\rho}{2R_0}\right] - \frac{4\mu}{\mu_0} \mathcal{T}(\mu, \chi)}. \tag{A11}$$

In particular, when the granular material is not vibrated, $\rho = 0$, so that

$$m^{\mathrm{eq}} = \begin{cases} \mathcal{T}(\mu, \chi), & \text{if} (\mu/\mu_0) \mathcal{T}(\mu, \chi) < 1; \\ \mu_0/\mu, & \text{if} (\mu/\mu_0) \mathcal{T}(\mu, \chi) \geq 1. \end{cases} \tag{A12}$$

In effect, the parameter μ_0, which originates from the proportionality between the mechanical noise strength Γ and the plastic work of deformation, sets of minimum flow stress when the granular material is not vibrated. But if $\rho \neq 0$, the system is unjammed.

Appendix B: Derivation of Equation (5) From (4)

The derivation of the full equation for the temporal evolution of χ, equation (5), from equation (4), involves identifying the physical elements such as Y/τ for the work rate of external vibrations and $\mathcal{K}$ for the entropy flow from the granular layer to the surroundings. It is largely parallel to that presented in *Lieou et al.* [2015], but we repeat it here for completeness.

We recognize that $\mathcal{K}$ ought to contain contributions from shearing, interparticle friction, and external vibration. Our strategy is to first determine $\mathcal{K}$ for frictionless grains and account for the effect of frictional contact between grains later. To this end, we observe that in the absence of frictional and vibrational noise, the only noise source having an effect on the granular layer would be that of shearing; as such, the steady state compactivity is determined entirely by the dimensionless shear rate $q \equiv \tau \dot{\gamma}^{\mathrm{pl}}$ to be $\hat{\chi}(q)$. Direct substitution of this into equation (4) yields

$$\mathcal{K} = \frac{W}{\hat{\chi}(q)}, \tag{B1}$$

where the dimensionless work rate $W = \tau \mu \dot{\gamma}^{\mathrm{pl}}$ is proportional to the mechanical noise strength Γ, to be discussed in greater detail afterward.

Next, if the granular layer is subject only to vibration but not shearing, the steady state compactivity is determined by the vibration intensity ρ alone, to be denoted by $\tilde{\chi}(\rho)$. In such a case, a similar procedure gives

$$\mathcal{K} = \frac{Y}{\tilde{\chi}(\rho)}. \tag{B2}$$

If the granular layer is both sheared and vibrated, the shear rate sets a time scale below which vibration cannot compete with shearing in causing the layer to explore different configurational states by generating STZs and rearranging the grains. Thus, we propose that

$$\mathcal{K}(\chi) = \frac{1}{\tau}\left[\frac{W}{\hat{\chi}(q)} + r\frac{Y}{\tilde{\chi}(\rho)}\right], \tag{B3}$$

where the parameter $r \equiv \exp(-q^2/\rho)$ determines the relative effects of shearing versus vibration: $r \to 0$ when q^2/ρ is large, and $r \to 1$ in the opposite limit.

If friction is present between the grains, we propose to modify the coupling coefficient $\mathcal{K}$ according to

$$\mathcal{K}(\chi) = \frac{1}{\tau}\left[\frac{W+F}{\hat{\chi}(q)} + r\frac{Y}{\tilde{\chi}(\rho)}\right], \tag{B4}$$

where F denotes the dissipation rate due to frictional contacts between grains. Then the equation of motion for χ, equation (4), reads

$$\epsilon_1\dot{\chi} = \frac{W+Y}{\tau} - \frac{1}{\tau}\left[\frac{W+F}{\hat{\chi}(q)} + r\frac{Y}{\tilde{\chi}(\rho)}\right]\chi. \tag{B5}$$

To proceed, it suffices to cast the quantities W, Y, and F in terms of the noise strengths. First, the mechanical noise strength Γ is proportional to the work dissipated per STZ [*Lieou et al.*, 2015]. Thus,

$$W = \Gamma\epsilon_0\mu_0\Lambda. \tag{B6}$$

Here the quantity μ_0, which can be interpreted as the minimum flow stress, is the same as the one introduced in the main sections of the paper; in fact, equation (B6) is the origin of this parameter. Next, we propose that the vibrational noise strength ρ is proportional to the work rate Y corresponding to external vibrations, so that

$$Y = A_0\rho \tag{B7}$$

for some dimensionless number A_0. Finally, the frictional dissipation ought to be proportional to the number of rearranging spots, and therefore the number of STZ's, in the granular medium. Therefore, the frictional noise strength ξ is given by

$$F = \xi\epsilon_0\mu_0\Lambda. \tag{B8}$$

Once we substitute equations (B6), (B7), and (B8) into (4), (5) follows.

Appendix C: Shear- and Vibration-Controlled Steady State Compactivities $\hat{\chi}(q)$ and $\tilde{\chi}(\rho)$

We introduced in section 2 the quantities $\hat{\chi}(q)$ and $\tilde{\chi}(\rho)$. The former denotes the steady state compactivity when a granular layer composed of smooth grains is sheared at a dimensionless strain rate q but not vibrated, while the latter denotes the steady state compactivity if an unsheared granular layer is vibrated at intensity ρ. As we noted in the main text, $\hat{\chi}(q)$ describes shear rate dilation; it approaches some constant $\hat{\chi}_0$ in the slow shear rate limit and diverges as $q \to \infty$. Motivated by the analogous quantity in the physics of amorphous solids, we choose to interpolate between the two limits using the inverse function [*Lieou et al.*, 2015]

$$q(\hat{\chi}) = q_0 \exp\left[-\frac{A}{\hat{\chi}} - \alpha_{\text{eff}}(\hat{\chi})\right], \tag{C1}$$

where

$$\alpha_{\text{eff}}(\hat{\chi}) = \left(\frac{\hat{\chi}_1}{\hat{\chi}-\hat{\chi}_0}\right)\exp\left(-3\frac{\hat{\chi}-\hat{\chi}_0}{\hat{\chi}_A-\hat{\chi}_0}\right). \tag{C2}$$

Throughout this paper, we have chosen the parameter values $\hat{\chi}_0 = 0.3$, $\hat{\chi}_1 = 0.02$, $\hat{\chi}_A = 0.33$, $A = 2$, and $q_0 = 2$, as was done in *Lieou et al.* [2014b, 2015].

Meanwhile, $\tilde{\chi}(\rho)$ is a decreasing function of increasing vibration intensity ρ, which reduces the thickness of the granular layer. For the purposes of this paper, we only consider vibration at several fixed, distinct intensities, that do not change continuously with time. Therefore, instead of proposing the full functional form for $\tilde{\chi}(\rho)$, it suffices for us to specify its values at the vibration intensities of interest, as in Figure 2b.

Acknowledgments
We thank Jean-Paul Ampuero and Ralph Archuleta for instructive discussions. This work was supported by NSF grants DMR0606092 and EAR-1345108, and the NSF/USGS Southern California Earthquake Center, funded by NSF Cooperative Agreement EAR-0529922 and USGS Cooperative Agreement 07HQAG0008, and the David and Lucile Packard Foundation. The data and codes for this paper are available by contacting the corresponding author.

References

Beroza, G. C., and S. Ide (2011), Slow earthquakes and nonvolcanic tremor, *Annu. Rev. Earth Planet. Sci.*, *39*(1), 271–296, doi:10.1146/annurev-earth-040809-152531.

Brace, W. F., and J. D. Byerlee (1966), Stick-slip as a mechanism for earthquakes, *Science*, *153*(3739), 990–992, doi:10.1126/science.153.3739.990.

Brace, W. F., and J. D. Byerlee (1970), California earthquakes: Why only shallow focus?, *Science*, *168*(3939), 1573–1575, doi:10.1126/science.168.3939.1573.

Brodsky, E. E., and S. G. Prejean (2005), New constraints on mechanisms of remotely triggered seismicity at Long Valley Caldera, *J. Geophys. Res.*, *110*, B04302, doi:10.1029/2004JB003211.

Daub, E. G., and J. M. Carlson (2009), Stick-slip instabilities and shear strain localization in amorphous materials, *Phys. Rev. E*, *80*, 066113, doi:10.1103/PhysRevE.80.066113.

Daub, E. G., and J. M. Carlson (2010), Friction, fracture, and earthquakes, *Annu. Rev. Condens. Matter Phys.*, *1*(1), 397–418, doi:10.1146/annurev-conmatphys-070909-104025.

Dijksman, J. A., G. H. Wortel, L. T. H. van Dellen, O. Dauchot, and M. van Hecke (2011), Jamming, yielding, and rheology of weakly vibrated granular media, *Phys. Rev. Lett.*, *107*, 108303, doi:10.1103/PhysRevLett.107.108303.

Dragert, H., K. Wang, and T. S. James (2001), A silent slip event on the deeper Cascadia subduction interface, *Science*, *292*(5521), 1525–1528, doi:10.1126/science.1060152.

Elbanna, A. E., and J. M. Carlson (2014), A two-scale model for sheared fault gouge: Competition between macroscopic disorder and local viscoplasticity, *J. Geophys. Res. Solid Earth*, *119*, 4841–4859, doi:10.1002/2014JB011001.

Falk, M. L., and J. Langer (2011), Deformation and failure of amorphous, solidlike materials, *Annu. Rev. Condens. Matter Phys.*, *2*(1), 353–373, doi:10.1146/annurev-conmatphys-062910-140452.

Falk, M. L., and J. S. Langer (1998), Dynamics of viscoplastic deformation in amorphous solids, *Phys. Rev. E*, *57*, 7192–7205, doi:10.1103/PhysRevE.57.7192.

Ferdowsi, B., M. Griffa, R. A. Guyer, P. A. Johnson, C. Marone, and J. Carmeliet (2014a), Three-dimensional discrete element modeling of triggered slip in sheared granular media, *Phys. Rev. E*, *89*, 042204, doi:10.1103/PhysRevE.89.042204.

Ferdowsi, B., M. Griffa, R. Guyer, P. Johnson, and J. Carmeliet (2014b), Effect of boundary vibration on the frictional behavior of a dense sheared granular layer, *Acta Mech.*, *225*(8), 2227–2237, doi:10.1007/s00707-014-1136-y.

Gomberg, J. (2010), Lessons from (triggered) tremor, *J. Geophys. Res.*, *115*, B10302, doi:10.1029/2009JB007011.

Griffa, M., E. G. Daub, R. A. Guyer, P. A. Johnson, C. Marone, and J. Carmeliet (2011), Vibration-induced slip in sheared granular layers and the micromechanics of dynamic earthquake triggering, *Europhys. Lett.*, *96*(1), 14001.

Griffa, M., B. Ferdowsi, R. A. Guyer, E. G. Daub, P. A. Johnson, C. Marone, and J. Carmeliet (2013), Influence of vibration amplitude on dynamic triggering of slip in sheared granular layers, *Phys. Rev. E*, *87*, 012205, doi:10.1103/PhysRevE.87.012205.

Hayman, N. W., L. Ducloue, K. L. Foco, and K. E. Daniels (2011), Granular controls on periodicity of stick-slip events: Kinematics and force-chains in an experimental fault, *Pure Appl. Geophys.*, *168*(12), 2239–2257, doi:10.1007/s00024-011-0269-3.

Ide, S. (2008), A Brownian walk model for slow earthquakes, *Geophys. Res. Lett.*, *35*, L17301, doi:10.1029/2008GL034821.

Itaba, S., and R. Ando (2011), A slow slip event triggered by teleseismic surface waves, *Geophys. Res. Lett.*, *38*, L21306, doi:10.1029/2011GL049593.

Johnson, P. A., H. Savage, M. Knuth, J. Gomberg, and C. Marone (2008), Effects of acoustic waves on stick-slip in granular media and implications for earthquakes, *Nature*, *451*, 57–60.

Johnson, P. A., B. Carpenter, M. Knuth, B. M. Kaproth, P.-Y. Le Bas, E. G. Daub, and C. Marone (2012), Nonlinear dynamical triggering of slow slip on simulated earthquake faults with implications to Earth, *J. Geophys. Res.*, *117*, B04310, doi:10.1029/2011JB008594.

Johnson, T., F. T. Wu, and C. H. Scholz (1973), Source parameters for stick-slip and for earthquakes, *Science*, *179*(4070), 278–280, doi:10.1126/science.179.4070.278.

Jop, P., Y. Forterre, and O. Pouliquen (2006), A constitutive law for dense granular flows, *Nature*, *447*, 727–730.

Kaproth, B. M., and C. Marone (2013), Slow earthquakes, preseismic velocity changes, and the origin of slow frictional stick-slip, *Science*, *341*(6151), 1229–1232, doi:10.1126/science.1239577.

Knight, J. B., C. G. Fandrich, C. N. Lau, H. M. Jaeger, and S. R. Nagel (1995), Density relaxation in a vibrated granular material, *Phys. Rev. E*, *51*, 3957–3963, doi:10.1103/PhysRevE.51.3957.

Lieou, C. K. C., A. E. Elbanna, and J. M. Carlson (2014a), Grain fragmentation in sheared granular flow: Weakening effects, energy dissipation, and strain localization, *Phys. Rev. E*, *89*, 022203, doi:10.1103/PhysRevE.89.022203.

Lieou, C. K. C., A. E. Elbanna, J. S. Langer, and J. M. Carlson (2014b), Shear flow of angular grains: Acoustic effects and nonmonotonic rate dependence of volume, *Phys. Rev. E*, *90*, 032204, doi:10.1103/PhysRevE.90.032204.

Lieou, C. K. C., A. E. Elbanna, J. S. Langer, and J. M. Carlson (2015), Stick-slip instabilities in sheared granular flow: The role of friction and acoustic vibrations, *Phys. Rev. E*, *92*, 022209, doi:10.1103/PhysRevE.92.022209.

Liu, Y., and J. R. Rice (2007), Spontaneous and triggered aseismic deformation transients in a subduction fault model, *J. Geophys. Res.*, *112*, B09404, doi:10.1029/2007JB004930.

Mair, K., and S. Abe (2011), Breaking up: Comminution mechanisms in sheared simulated fault gouge, *Pure Appl. Geophys.*, *168*(12), 2277–2288, doi:10.1007/s00024-011-0266-6.

Manning, M. L., J. S. Langer, and J. M. Carlson (2007), Strain localization in a shear transformation zone model for amorphous solids, *Phys. Rev. E*, *76*, 056106, doi:10.1103/PhysRevE.76.056106.

Manning, M. L., E. G. Daub, J. S. Langer, and J. M. Carlson (2009), Rate-dependent shear bands in a shear-transformation-zone model of amorphous solids, *Phys. Rev. E*, *79*, 016110, doi:10.1103/PhysRevE.79.016110.

Marsan, D., and O. Lengline (2008), Extending earthquakes' reach through cascading, *Science*, *319*(5866), 1076–1079, doi:10.1126/science.1148783.

Nowak, E. R., J. B. Knight, E. Ben-Naim, H. M. Jaeger, and S. R. Nagel (1998), Density fluctuations in vibrated granular materials, *Phys. Rev. E*, *57*, 1971–1982, doi:10.1103/PhysRevE.57.1971.

Obara, K. (2002), Nonvolcanic deep tremor associated with subduction in southwest Japan, *Science*, *296*(5573), 1679–1681, doi:10.1126/science.1070378.

Obara, K., H. Hirose, F. Yamamizu, and K. Kasahara (2004), Episodic slow slip events accompanied by non-volcanic tremors in southwest Japan subduction zone, *Geophys. Res. Lett.*, *31*, L23602, doi:10.1029/2004GL020848.

Rogers, G., and H. Dragert (2003), Episodic tremor and slip on the cascadia subduction zone: The chatter of silent slip, *Science*, *300*(5627), 1942–1943, doi:10.1126/science.1084783.

Rubin, A. M. (2008), Episodic slow slip events and rate-and-state friction, *J. Geophys. Res.*, *113*, B11414, doi:10.1029/2008JB005642.
Rubinstein, J. L., D. R. Shelly, and W. L. Ellsworth (2010), Non-volcanic tremor: A window into the roots of fault zones, in *New Frontiers in Integrated Solid Earth Sciences, Int. Year of Planet Earth*, edited by S. Cloetingh and J. Negendank, pp. 287–314, Springer, Netherlands.
Sammis, C., G. King, and R. Biegel (1987), The kinematics of gouge deformation, *Pure Appl. Geophys.*, *125*(5), 777–812, doi:10.1007/BF00878033.
Scholz, C. H. (2010), Large earthquake triggering, clustering, and the synchronization of faults, *Bull. Seismol. Soc. Am.*, *100*(3), 901–909, doi:10.1785/0120090309.
Tordesillas, A., J. Zhang, and R. Behringer (2009), Buckling force chains in dense granular assemblies: Physical and numerical experiments, *Geomech. Geoeng.*, *4*(1), 3–16, doi:10.1080/17486020902767347.
van der Elst, N. J., E. E. Brodsky, P.-Y. Le Bas, and P. A. Johnson (2012), Auto-acoustic compaction in steady shear flows: Experimental evidence for suppression of shear dilatancy by internal acoustic vibration, *J. Geophys. Res.*, *117*, B09314, doi:10.1029/2011JB008897.
Wei, M., Y. Liu, Y. Kaneko, J. J. McGuire, and R. Bilham (2015), Dynamic triggering of creep events in the Salton Trough, Southern California by regional earthquakes constrained by geodetic observations and numerical simulations, *Earth Planet. Sci. Lett.*, *427*, 1–10, doi:10.1016/j.epsl.2015.06.04.
Wortel, G. H., J. A. Dijksman, and M. van Hecke (2014), Rheology of weakly vibrated granular media, *Phys. Rev. E*, *89*, 012202, doi:10.1103/PhysRevE.89.012202.
Zigone, D., et al. (2012), Triggering of tremors and slow slip event in Guerrero, Mexico, by the 2010 M_w 8.8 Maule, Chile, earthquake, *J. Geophys. Res.*, *117*, B09304, doi:10.1029/2012JB009160.